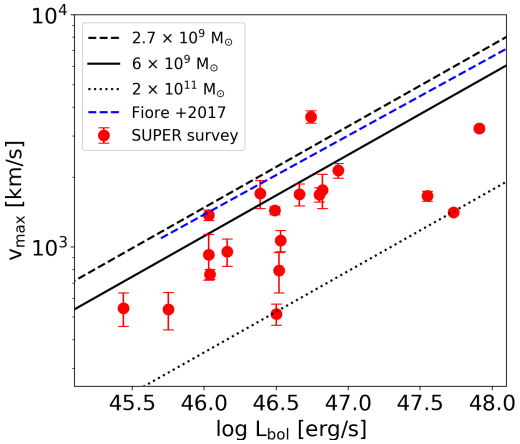

Fig. 13. Maximum velocity, $v_{\rm max}$, defined in Sect. 6, versus AGN bolometric luminosity. The red circles represent the SUPER targets, the dashed blue line shows the best fit relation for literature data compiled in Fiore et al. (2017). The black curves are the Menci et al. (2019) predictions for the shock velocity (approximated here by the measured $v_{\rm max}$) versus AGN luminosity for galaxies. The three curves correspond to molecular gas masses of $2.7 \times 10^9\ M_\odot$, $6 \times 10^9\ M_\odot$ and $2 \times 10^{11}\ M_\odot$, respectively. More details are given in Sect. 6.

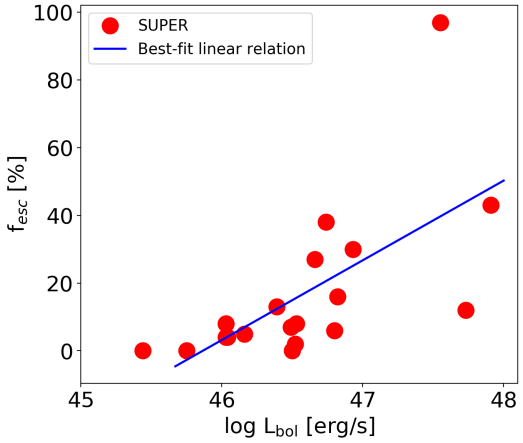

Fig. 14. Escape fraction as a function of the bolometric luminosity of the AGN for the Type 1 sample presented in this paper. The escape velocity is calculated for a distance of 2 kpc from Eq. (5). The blue curve shows the best-fit relation.

the AGN location (see Rupke et al. 2002):

$$V_{\rm esc} = \sqrt{2} V_c \left[1 + ln\left(\frac{r_{\rm max}}{r}\right)\right]^{1/2}, \quad (5)$$

where $r_{\rm max}$ is the extent of the dark matter halo (assumed ~100 kpc here) and V_c is the circular velocity of the galaxy, assumed to be 300 km s^{-1} as in Eq. (4) from the Tully-Fischer relation for the range of stellar mass in SUPER galaxies (see Cresci et al. 2009). At 2 kpc, which is roughly the spatial resolution of the H-band SINFONI observations, the escape velocity calculated using Eq. (5) is on average ~950 km s^{-1}. We then estimated the escape fraction of ionised gas as the ratio between the flux of the [O III] λ5007 channels in the integrated spectra with $|v| > V_{\rm esc}$ and the total flux of the [O III] λ5007 line. The escape fraction of the ionised gas calculated for the Type 1 SUPER sample presented in this paper is reported in Table 4. For most galaxies, $\lesssim$10% of the outflowing ionised gas has the ability to escape the host galaxy, while the rest of the gas is expected to re-accrete back onto the host galaxy. The highest escape fractions of ~43% and ~97% are observed in J1333+1649 and J1441+0454, which are also the targets with high bolometric luminosity. We note that in J1441+0454, the exceptionally high escape fraction is a result of the extremely blueshifted [O III] profile, which is also blended with the iron emission as explained in Sect. 5.1. Figure 14 shows the escape fraction as a function of the bolometric luminosity, which suggests a positive correlation between the two quantities, but with a large scatter. The Pearson correlation coefficient between the escape fraction and the bolometric luminosity is 0.64 with a null hypothesis probability of ~0.2%. Although the correlation is relatively weak compared to the $w_{80} - L_{\rm bol}$ relation in Fig. 12, the data might suggest that outflows hosted in high luminosity AGN have a higher fraction of escaping gas.

We also note that SINFONI data only trace the ionised phase of the outflow, while a large fraction of the outflow might be present in the molecular gas phase (e.g. Cicone et al. 2018; Fluetsch et al. 2019). Therefore, follow-up studies in other gas phases such as the warm and cold molecular phase and neutral gas phase are required to complete the picture of the effects of radiation pressure on the ISM of the galaxies.

7. Summary and conclusions

We present near-infrared IFU spectroscopy for 21 X-ray selected Type 1 AGN from the SUPER survey (half of the survey size). We traced and characterised the velocity and extension of the ionised gas and its outflow component in the NLR using the [O III] λ5007 transition. The main conclusions from the work presented in this paper are summarised below.

1. Using a cut on the non-parametric velocity width, $w_{80} > 600$ km s^{-1}, in the integrated spectra, we find that all the Type 1 AGN in the SUPER survey show the presence of ionised outflows. We consider the selected threshold in w_{80} a conservative choice, based on the very diverse distributions of low-z and high-z mass matched sample of star forming galaxies compared to the w_{80} distribution of AGN host galaxies (Sect. 5.1, Fig. 3). We also confirm a strong linear correlation between the [O III] luminosity and the X-ray luminosity, as previously observed in the literature (Sect. 5.1, Fig. 4).
2. Using three different methods (COG analysis, half-light radii, and the PSF-subtraction method), we find evidence of kiloparsec-scale extended ionised gas emission in seven out of the 11 targets for which [O III] is detected at an $S/N > 5$ in the integrated spectrum (Sect. 5.2, Figs. 5 and 6). Flux and velocity maps of these resolved targets reveal outflows extended to ~6 kiloparsec (quantified by D_{600} value, Table 4 and Figs. 7 and 8), with indications of redshifted outflows in three objects (cid_346, J1333+1649, and S82X1905).
3. We used the spectroastrometry method to determine the distance of the bulk of the gas moving at a given velocity. We find that the high-velocity outflowing gas ($|v| > 600$ km s^{-1}) is contained in the central ~1 kpc for ~80% of the targets for which the spectroastrometry analysis was performed (Sect. 5.4). For two objects (cid_346 and S82X1905) the bulk motion of high-velocity gas is extended to ~3 kpc.
4. We explored a range of plausible assumptions on the physical properties of the outflow (its geometry, velocity, and radius) and of the outflowing gas (i.e. its electron density) and report the range of derived mass outflow rates for each target (Sect. 5.5). The mass outflow rates of the Type 1 sample are in the range of ~0.01–1000 $M_\odot$ yr^{-1} (Table 4). After factoring in the systematic uncertainties in the outflow models, these outflow rates seem to correlate with the bolometric luminosity of the AGN.

5. The non-parametric velocity, w_{80}, strongly correlates with the X-ray luminosity, $L_X(2-10\,\mathrm{keV})$, and the bolometric luminosity of the central super massive black hole (Fig. 12). The correlation is relatively weak for w_{80} versus M_{BH} (or L_{Edd}). The maximum velocity versus bolometric luminosity plot for the SUPER sample agrees with model predictions for an AGN-driven shock driving an outflow through a galaxy disc (Fig. 13).
6. For most galaxies, <10% of the outflows in the ionised gas have the potenial to escape the gravitational potential of the host galaxy. The escape fraction also increases with the bolometric luminosity of the AGN (Fig. 14).

While this paper focused on presenting the ionised gas kinematics of the Type 1 sample, an upcoming publication will present the SINFONI and ALMA results for the overall (Type 1 and Type 2) AGN SUPER sample. The different types of morphology of the ionised gas and the associated outflows presented in this paper clearly show the advantages of performing high spatial resolution observations. Even better spatial and spectral resolution and higher sensitivity is expected with future facilities such as ELT/HARMONI. Such observations will enable us to resolve the extended redshifted and blueshifted outflowing gas, which might reveal sub-structures within the outflow, and trace the radial evolution of the outflowing gas, which is certainly not possible at $z \sim 2$ with today's instrumentation. Finally, we are currently limited to studying ionised outflows from the ground up to $z \approx 4$, observing the [O III] line in the K-band. With the IFU capabilities of NIRSpec on-board the JWST, a study similar to the one presented in this paper could be performed with comparable resolution at $z > 4$ and will allow us to further constrain the importance of AGN feedback at earlier comic epochs.

Acknowledgements. We thank the referee for the useful and constructive comments. We thank Michele Cirasuolo, Alice Concas and Dominika Wylezalek for providing the comparison data for the w_{80} distribution. M. P. is supported by the Programa Atracción de Talento de la Comunidad de Madrid via grant 2018-T2/TIC-11715. Based on observations collected at the European organisation for Astronomical Research in the Southern Hemisphere under ESO program 196.A-0377.

References

Aalto, S., Muller, S., König, S., et al. 2019, A&A, 627, A147
Aladro, R., König, S., Aalto, S., et al. 2018, A&A, 617, A20
Alexander, D. M., Swinbank, A. M., Smail, I., McDermid, R., & Nesvadba, N. P. H. 2010, MNRAS, 402, 2211
Bae, H.-J., Woo, J.-H., Karouzos, M., et al. 2017, ApJ, 837, 91
Baron, D., & Netzer, H. 2019, MNRAS, 486, 4290
Batiste, M., Bentz, M. C., Raimundo, S. I., Vestergaard, M., & Onken, C. A. 2017, ApJ, 838, L10
Begelman, M. C. 2003, Science, 300, 1898
Bennert, N., Falcke, H., Schulz, H., Wilson, A. S., & Wills, B. J. 2002, ApJ, 574, L105
Bischetti, M., Piconcelli, E., Vietri, G., et al. 2017, A&A, 598, A122
Boroson, T. A., & Green, R. F. 1992, ApJS, 80, 109
Bouché, N., Murphy, M. T., Kacprzak, G. G., et al. 2013, Science, 341, 50
Brandt, W. N., & Alexander, D. M. 2015, A&ARv, 23, 1
Brusa, M., Bongiorno, A., Cresci, G., et al. 2015, MNRAS, 446, 2394
Brusa, M., Perna, M., Cresci, G., et al. 2016, A&A, 588, A58
Brusa, M., Cresci, G., Daddi, E., et al. 2018, A&A, 612, A29
Bryant, J. J., Owers, M. S., Robotham, A. S. G., et al. 2015, MNRAS, 447, 2857
Bundy, K., Bershady, M. A., Law, D. R., et al. 2015, ApJ, 798, 7
Caglar, T., Burtscher, L., Brandl, B., et al. 2020, A&A, 634, A114
Cano-Díaz, M., Maiolino, R., Marconi, A., et al. 2012, A&A, 537, L8
Carniani, S., Marconi, A., Maiolino, R., et al. 2015, A&A, 580, A102
Carniani, S., Marconi, A., Maiolino, R., et al. 2016, A&A, 591, A28
Cazzoli, S., Arribas, S., Maiolino, R., & Colina, L. 2016, A&A, 590, A125
Choi, E., Naab, T., Ostriker, J. P., Johansson, P. H., & Moster, B. P. 2014, MNRAS, 442, 440
Cicone, C., Brusa, M., Ramos Almeida, C., et al. 2018, Nat. Astron., 2, 176
Cicone, C., Maiolino, R., Aalto, S., Muller, S., & Feruglio, C. 2020, A&A, 633, A163
Circosta, C., Mainieri, V., Padovani, P., et al. 2018, A&A, 620, A82
Civano, F., Marchesi, S., Comastri, A., et al. 2016, ApJ, 819, 62
Coatman, L., Hewett, P. C., Banerji, M., et al. 2019, MNRAS, 486, 5335
Concas, A., Popesso, P., Brusa, M., Mainieri, V., & Thomas, D. 2019, A&A, 622, A188
Crenshaw, D. M., Kraemer, S. B., Schmitt, H. R., et al. 2010, AJ, 139, 871
Cresci, G., Hicks, E. K. S., Genzel, R., et al. 2009, ApJ, 697, 115
Cresci, G., Mainieri, V., Brusa, M., et al. 2015, ApJ, 799, 82
Curran, S. J. 2019, MNRAS, 484, 3911
Curti, M., Maiolino, R., Cirasuolo, M., et al. 2020, MNRAS, 492, 821
Davies, R. I. 2007, MNRAS, 375, 1099
Davies, R. I., Maciejewski, W., Hicks, E. K. S., et al. 2014, ApJ, 792, 101
Davies, R. L., Förster Schreiber, N. M., Übler, H., et al. 2019, ApJ, 873, 122
Davies, R., Baron, D., Shimizu, T., et al. 2020a, MNRAS, 498, 4150
Davies, R. L., Schreiber, N. M. F., Lutz, D., et al. 2020b, ApJ, 894, 28
Dempsey, R., & Zakamska, N. L. 2018, MNRAS, 477, 4615
den Brok, M., Carollo, C. M., Erroz-Ferrer, S., et al. 2020, MNRAS, 491, 4089
Dimitrijević, M. S., Popović, L. Č., Kovačević, J., Dačić, M., & Ilić, D. 2007, MNRAS, 374, 1181
Eisenhauer, F., Abuter, R., Bickert, K., et al. 2003, in Instrument Design and Performance for Optical/Infrared Ground-based Telescopes, eds. M. Iye, A. F. M. Moorwood, et al., SPIE Conf. Ser., 4841, 1548
Emonts, B. H. C., Colina, L., Piqueras-López, J., et al. 2017, A&A, 607, A116
Faucher-Giguère, C.-A., & Quataert, E. 2012, MNRAS, 425, 605
Feruglio, C., Ferrara, A., Bischetti, M., et al. 2017, A&A, 608, A30
Fiore, F., Feruglio, C., Shankar, F., et al. 2017, A&A, 601, A143
Fluetsch, A., Maiolino, R., Carniani, S., et al. 2019, MNRAS, 483, 4586
Förster Schreiber, N. M., Renzini, A., Mancini, C., et al. 2018, ApJS, 238, 21
Förster Schreiber, N. M., Übler, H., Davies, R. L., et al. 2019, ApJ, 875, 21
Fruchter, A. S., & Hook, R. N. 2002, PASP, 114, 144
Gallagher, R., Maiolino, R., Belfiore, F., et al. 2019, MNRAS, 485, 3409
García-Burillo, S., Combes, F., Usero, A., et al. 2014, A&A, 567, A125
Gebhardt, K., Bender, R., Bower, G., et al. 2000, ApJ, 539, L13
Georgakakis, A., & Nandra, K. 2011, MNRAS, 414, 992
Hainline, K. N., Hickox, R. C., Greene, J. E., et al. 2014, ApJ, 787, 65
Harrison, C. M., Alexander, D. M., Swinbank, A. M., et al. 2012, MNRAS, 426, 1073
Harrison, C. M., Alexander, D. M., Mullaney, J. R., & Swinbank, A. M. 2014, MNRAS, 441, 3306
Harrison, C. M., Alexander, D. M., Mullaney, J. R., et al. 2016, MNRAS, 456, 1195
Harrison, C. M., Costa, T., Tadhunter, C. N., et al. 2018, Nat. Astron., 2, 198
Hill, M. J., & Zakamska, N. L. 2014, MNRAS, 439, 2701
Hopkins, P. F., Torrey, P., Faucher-Giguère, C.-A., Quataert, E., & Murray, N. 2016, MNRAS, 458, 816
Husemann, B., Wisotzki, L., Sánchez, S. F., & Jahnke, K. 2013, A&A, 549, A43
Husemann, B., Jahnke, K., Sánchez, S. F., et al. 2014, MNRAS, 443, 755
Husemann, B., Scharwächter, J., Bennert, V. N., et al. 2016, A&A, 594, A44
Husemann, B., Davis, T. A., Jahnke, K., et al. 2017, MNRAS, 470, 1570
Husemann, B., Scharwächter, J., Davis, T. A., et al. 2019, A&A, 627, A53
Ishibashi, W., & Fabian, A. C. 2016, MNRAS, 457, 2864
Ishibashi, W., Fabian, A. C., & Reynolds, C. S. 2019, MNRAS, 486, 2210
Jahnke, K., Wisotzki, L., Sánchez, S. F., et al. 2004, Astron. Nachr., 325, 128
Kakkad, D., Mainieri, V., Padovani, P., et al. 2016, A&A, 592, A148
Kakkad, D., Groves, B., Dopita, M., et al. 2018, A&A, 618, A6
Karouzos, M., Woo, J.-H., & Bae, H.-J. 2016, ApJ, 819, 148
King, A. 2003, ApJ, 596, L27
King, A., & Pounds, K. 2015, ARA&A, 53, 115
Krug, H. B., Rupke, D. S. N., & Veilleux, S. 2010, ApJ, 708, 1145
LaMassa, S. M., Urry, C. M., Cappelluti, N., et al. 2016, ApJ, 817, 172
Läsker, R., Greene, J. E., Seth, A., et al. 2016, ApJ, 825, 3
Leighly, K. M. 1999, ApJS, 125, 317
Leung, G. C. K., Coil, A. L., Aird, J., et al. 2019, ApJ, 886, 11
Liu, G., Zakamska, N. L., Greene, J. E., Nesvadba, N. P. H., & Liu, X. 2013, MNRAS, 436, 2576
Liu, Z., Merloni, A., Georgakakis, A., et al. 2016, MNRAS, 459, 1602
Luo, B., Brandt, W. N., Xue, Y. Q., et al. 2017, ApJS, 228, 2
Madau, P., & Dickinson, M. 2014, ARA&A, 52, 415
Magorrian, J., Tremaine, S., Richstone, D., et al. 1998, AJ, 115, 2285
Maiolino, R., Russell, H. R., Fabian, A. C., et al. 2017, Nature, 544, 202
Martocchia, S., Piconcelli, E., Zappacosta, L., et al. 2017, A&A, 608, A51
May, D., Rodríguez-Ardila, A., Prieto, M. A., et al. 2018, MNRAS, 481, L105
McElroy, R., Croom, S. M., Pracy, M., et al. 2015, MNRAS, 446, 2186
Menci, N., Fiore, F., Puccetti, S., & Cavaliere, A. 2008, ApJ, 686, 219

Menci, N., Fiore, F., Feruglio, C., et al. 2019, ApJ, 877, 74
Menzel, M. L., Merloni, A., Georgakakis, A., et al. 2016, MNRAS, 457, 110
Michiyama, T., Iono, D., Sliwa, K., et al. 2018, ApJ, 868, 95
Müller-Sánchez, F., Prieto, M. A., Hicks, E. K. S., et al. 2011, ApJ, 739, 69
Muratov, A. L., Kereš, D., Faucher-Giguère, C.-A., et al. 2015, MNRAS, 454, 2691
Nesvadba, N. P. H., Lehnert, M. D., Eisenhauer, F., et al. 2006, ApJ, 650, 693
Nesvadba, N. P. H., De Breuck, C., Lehnert, M. D., Best, P. N., & Collet, C. 2017, A&A, 599, A123
Nims, J., Quataert, E., & Faucher-Giguère, C.-A. 2015, MNRAS, 447, 3612
Padovani, P., Alexander, D. M., Assef, R. J., et al. 2017, A&A Rev., 25, 2
Perna, M., Brusa, M., Cresci, G., et al. 2015, A&A, 574, A82
Perna, M., Lanzuisi, G., Brusa, M., Cresci, G., & Mignoli, M. 2017, A&A, 606, A96
Perna, M., Cresci, G., Brusa, M., et al. 2019, A&A, 623, A171
Perrotta, S., Hamann, F., Zakamska, N. L., et al. 2019, MNRAS, 488, 4126
Petric, A. O., Armus, L., Flagey, N., et al. 2018, AJ, 156, 295
Radovich, M., Poggianti, B., Jaffé, Y. L., et al. 2019, MNRAS, 486, 486
Rakshit, S., & Woo, J.-H. 2018, ApJ, 865, 5
Revalski, M., Dashtamirova, D., Crenshaw, D. M., et al. 2018, ApJ, 867, 88
Riffel, R. A., Storchi-Bergmann, T., & Winge, C. 2013, MNRAS, 430, 2249
Riffel, R. A., Storchi-Bergmann, T., & Riffel, R. 2015, MNRAS, 451, 3587
Riffel, R. A., Zakamska, N. L., & Riffel, R. 2020, MNRAS, 491, 1518
Roberts-Borsani, G. W. 2020, MNRAS, 494, 4266
Rodríguez-Ardila, A., Binette, L., Pastoriza, M. G., & Donzelli, C. J. 2000, ApJ, 538, 581
Rupke, D. S. N., & Veilleux, S. 2011, ApJ, 729, L27
Rupke, D. S. N., & Veilleux, S. 2013, ApJ, 768, 75
Rupke, D. S., Veilleux, S., & Sanders, D. B. 2002, ApJ, 570, 588
Rupke, D. S. N., Gültekin, K., & Veilleux, S. 2017, ApJ, 850, 40
Sánchez, S. F., Kennicutt, R. C., Gil de Paz, A., et al. 2012, A&A, 538, A8
Scholtz, J., Harrison, C. M., Rosario, D. J., et al. 2020, MNRAS, 492, 3194
Schutte, Z., Reines, A. E., & Greene, J. E. 2019, ApJ, 887, 245
Serafinelli, R., Tombesi, F., Vagnetti, F., et al. 2019, A&A, 627, A121
Shankar, F., Weinberg, D. H., & Miralda-Escudé, J. 2009, ApJ, 690, 20
Shimizu, T. T., Davies, R. I., Lutz, D., et al. 2019, MNRAS, 490, 5860
Skrutskie, M. F., Cutri, R. M., Stiening, R., et al. 2006, AJ, 131, 1163
Steidel, C. C., Erb, D. K., Shapley, A. E., et al. 2010, ApJ, 717, 289
Storey, P. J., & Zeippen, C. J. 2000, MNRAS, 312, 813
Stott, J. P., Swinbank, A. M., Johnson, H. L., et al. 2016, MNRAS, 457, 1888
Swinbank, A. M., Harrison, C. M., Tiley, A. L., et al. 2019, MNRAS, 487, 381
Tacconi, L. J., Genzel, R., & Sternberg, A. 2020, ARA&A, submitted [arXiv:2003.06245]
Tadhunter, C., Morganti, R., Rose, M., Oonk, J. B. R., & Oosterloo, T. 2014, Nature, 511, 440
Thomas, A. D., Dopita, M. A., Shastri, P., et al. 2017, ApJS, 232, 11
Tsuzuki, Y., Kawara, K., Yoshii, Y., et al. 2006, ApJ, 650, 57
Vayner, A., Wright, S. A., Murray, N., et al. 2017, ApJ, 851, 126
Veilleux, S., Rupke, D. S. N., & Swaters, R. 2009, ApJ, 700, L149
Veilleux, S., Maiolino, R., Bolatto, A. D., & Aalto, S. 2020, A&ARv, 28, 2
Venturi, G., Nardini, E., Marconi, A., et al. 2018, A&A, 619, A74
Véron-Cetty, M. P., Joly, M., & Véron, P. 2004, A&A, 417, 515
Vietri, G., Piconcelli, E., Bischetti, M., et al. 2018, A&A, 617, A81
Villar-Martín, M., Arribas, S., Emonts, B., et al. 2016, MNRAS, 460, 130
Wagner, A. Y., Umemura, M., & Bicknell, G. V. 2013, ApJ, 763, L18
Whitaker, K. E., Rigby, J. R., Brammer, G. B., et al. 2014, ApJ, 790, 143
Wilkins, S. M., Lovell, C. C., & Stanway, E. R. 2019, MNRAS, 490, 5359
Wisnioski, E., Förster Schreiber, N. M., Fossati, M., et al. 2019, ApJ, 886, 124
Wylezalek, D., Zakamska, N. L., Liu, G., & Obied, G. 2016, MNRAS, 457, 745
Wylezalek, D., Flores, A. M., Zakamska, N. L., Greene, J. E., & Riffel, R. A. 2020, MNRAS, 492, 4680
Zakamska, N. L., & Greene, J. E. 2014, MNRAS, 442, 784
Zakamska, N. L., Hamann, F., Pâris, I., et al. 2016, MNRAS, 459, 3144
Zappacosta, L., Piconcelli, E., Giustini, M., et al. 2020, A&A, 635, L5
Zschaechner, L. K., Bolatto, A. D., Walter, F., et al. 2018, ApJ, 867, 111
Zubovas, K. 2018, MNRAS, 479, 3189
Zubovas, K., & King, A. 2012, ApJ, 745, L34
Zubovas, K., & Nayakshin, S. 2014, MNRAS, 440, 2625

Appendix A: Integrated *H*-band spectra and [O III] channel maps of the Type 1 SUPER sample

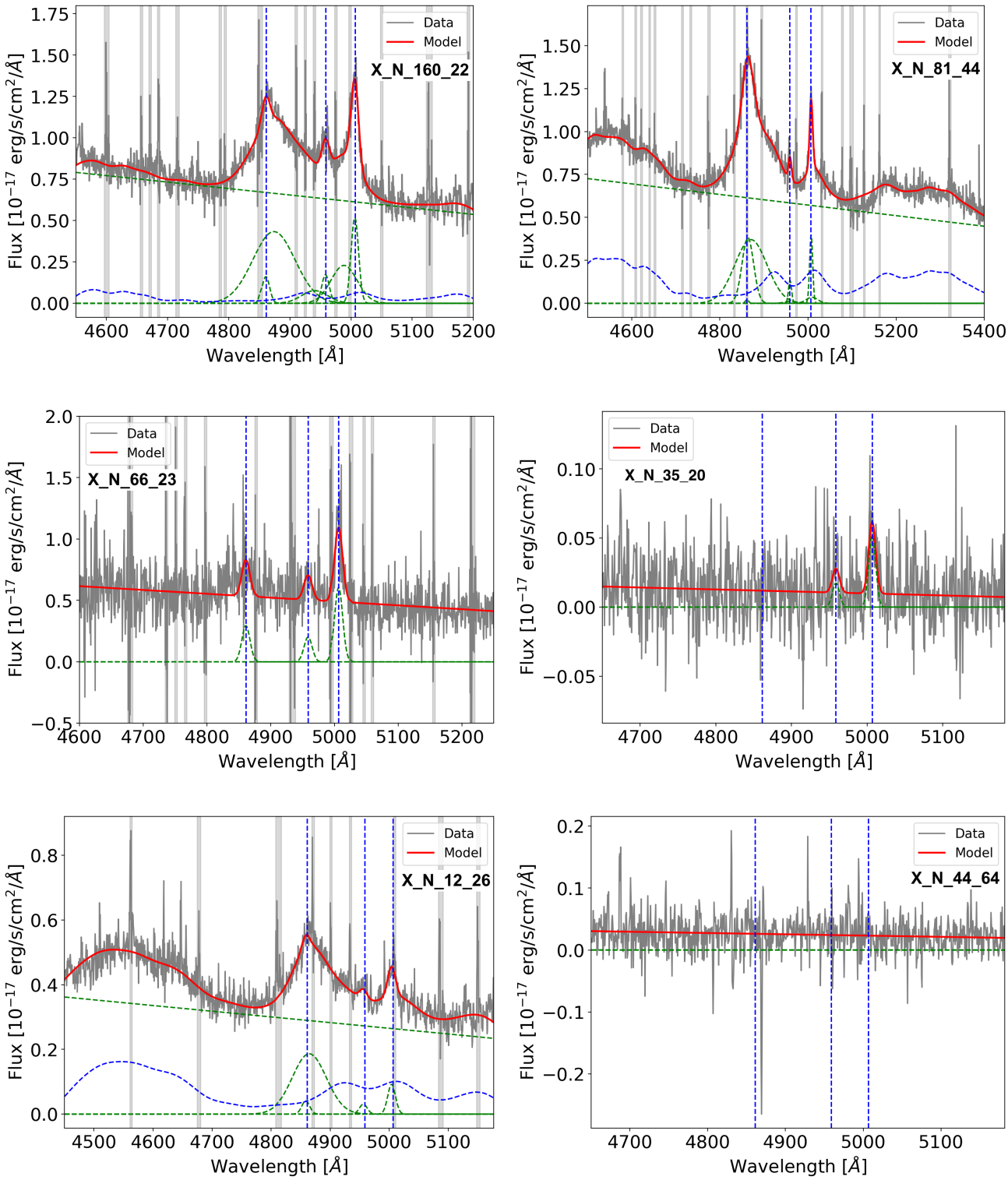

Fig. A.1. Integrated *H*-band spectrum of SUPER targets X_N_160_22, X_N_81_44, X_N_66_23, X_N_35_20, X_N_12_26, and X_N_44_64. The grey curve shows the observed spectrum, the red curve shows the reproduced overall emission line model, the blue dashed curve shows the iron emission, and the dashed green curves show the continuum emission and the individual Gaussian components (narrow, broad, and BLR) used to reproduce the profiles of various emission lines. The blue vertical lines indicate the locations of Hβ, [O III] λ4959, and [O III] λ5007. The vertical grey regions mark the channels with strong skylines, which were masked during the fitting procedure. The *X*-axis shows the rest frame wavelength after correcting for the redshift of the target and the *Y*-axis shows the observed flux.

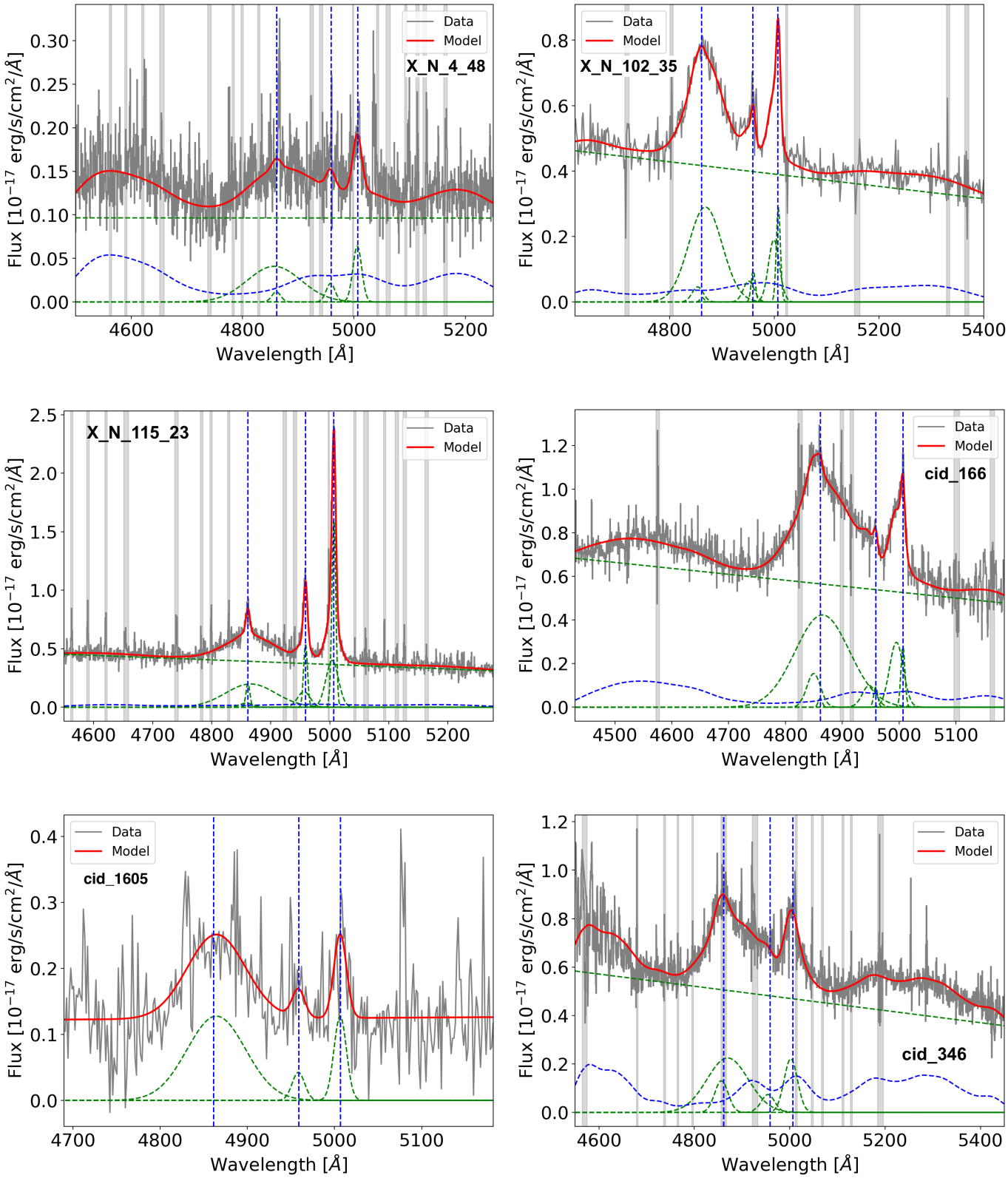

Fig. A.2. Same as Fig. A.1 for X_N_4_48, X_N_102_35, X_N_115_23, cid_166, cid_1605, and cid_346.

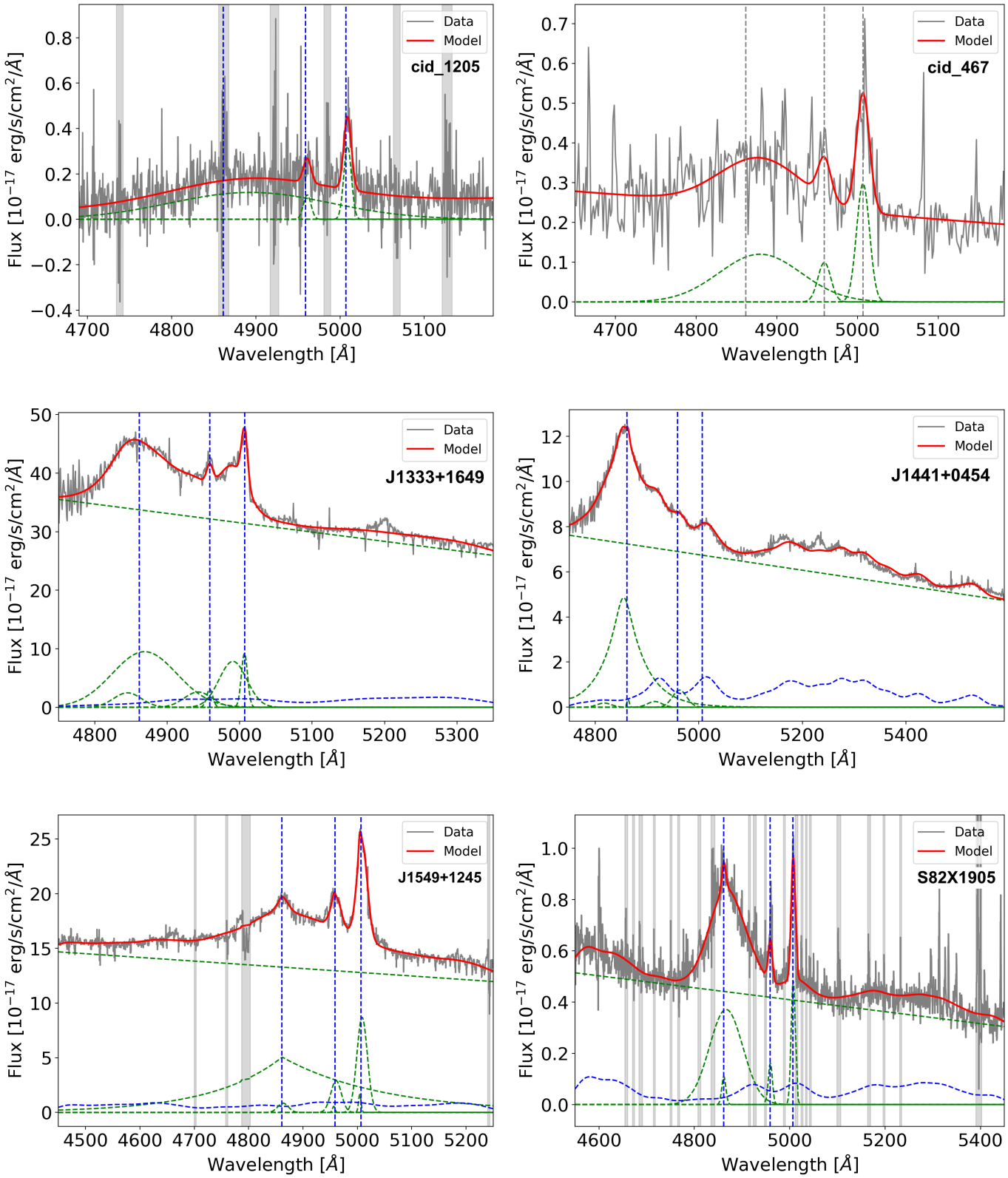

Fig. A.3. Same as Fig. A.1 for cid_1205, cid_467, J1333+1649, J1441+0454, J1549+1245, and S82X1905.

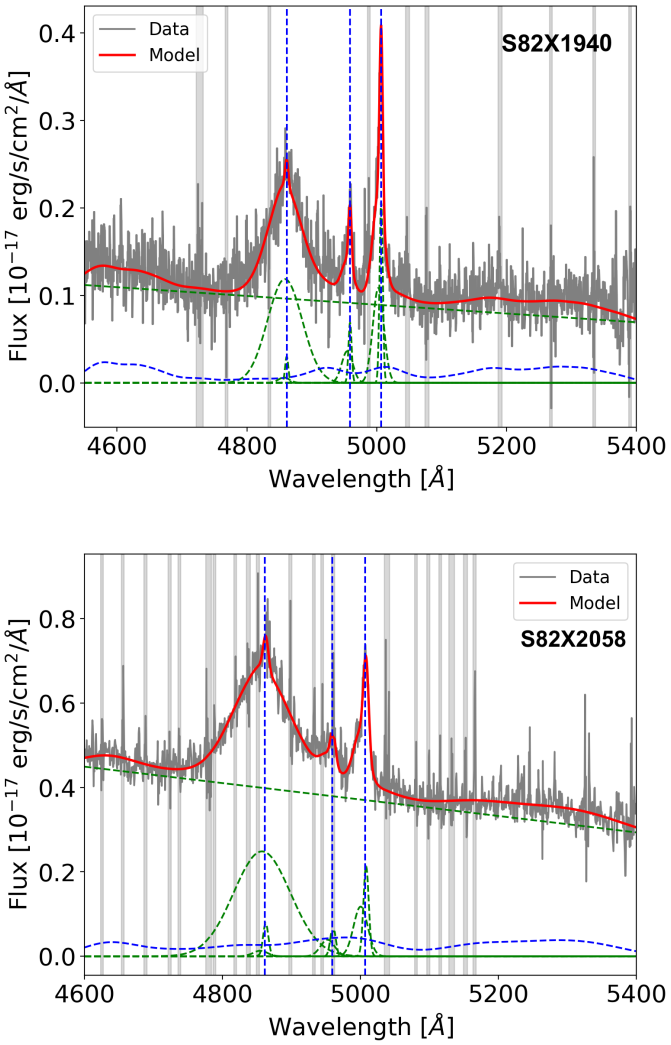

Fig. A.4. Same as Fig. A.1 for S82X1940 and S82X2058.

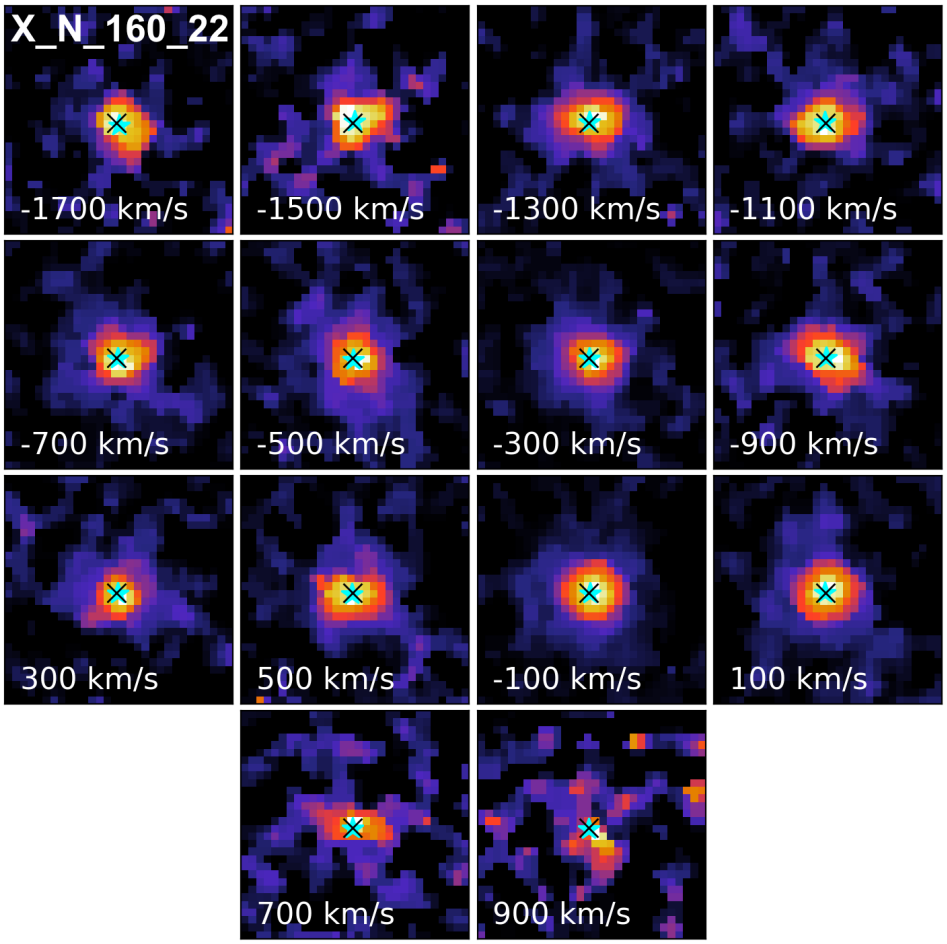

Fig. A.5. 1.5″ × 1.5″ [O III] λ5007 channel maps of SUPER target X_N_160_22 at different velocity slices, after subtracting the Hβ, [O III] λ4959, and iron models from the raw cube. Each velocity slice is 200 km s^{-1} wide, and the displayed value is the centre velocity of the respective channel. The black cross marks the location of the *H*-band continuum peak, used as a proxy for the AGN position. North is up and east is left.

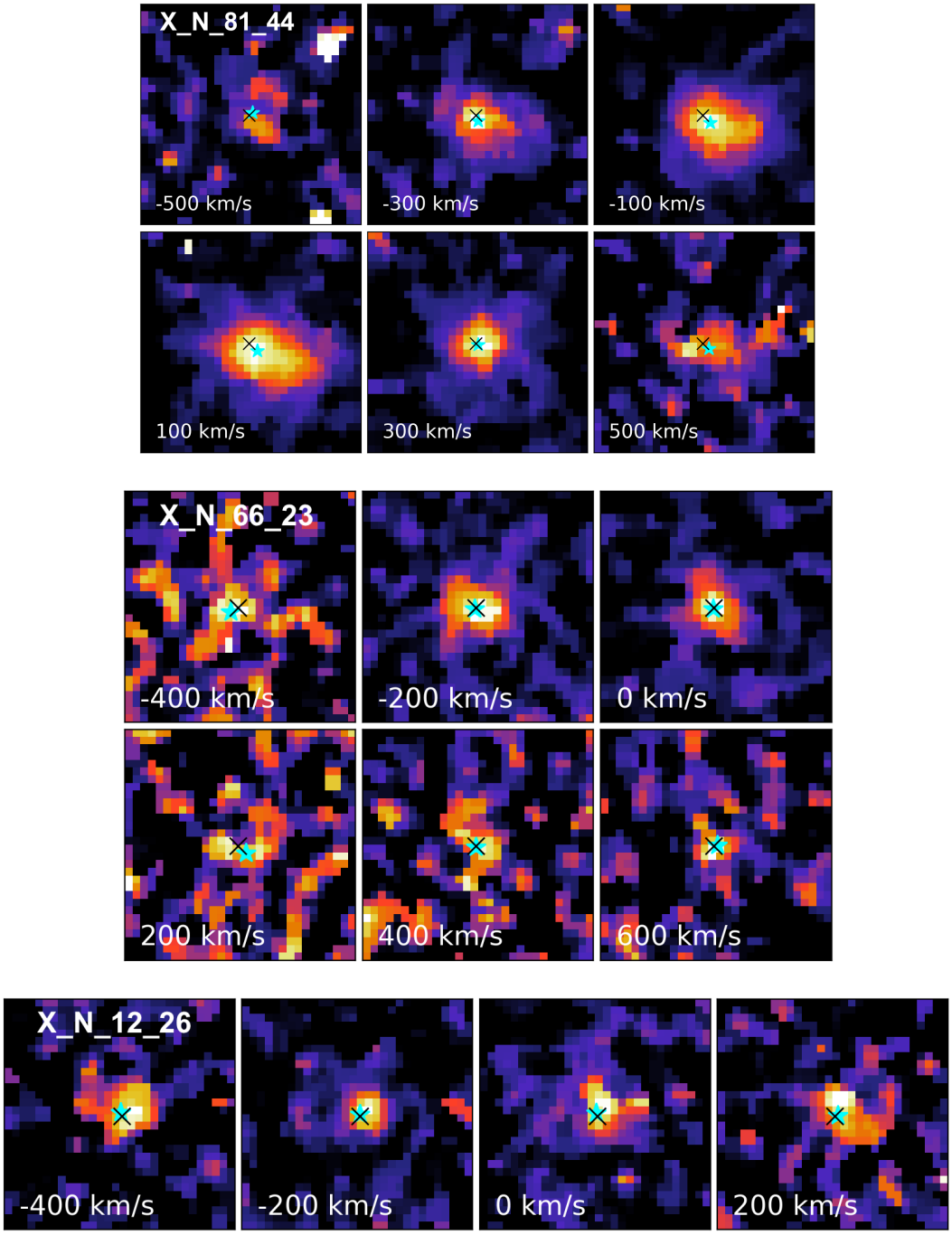

Fig. A.6. Same as in Fig. A.5 for X_N_81_44, X_N_66_23 and X_N_12_26.

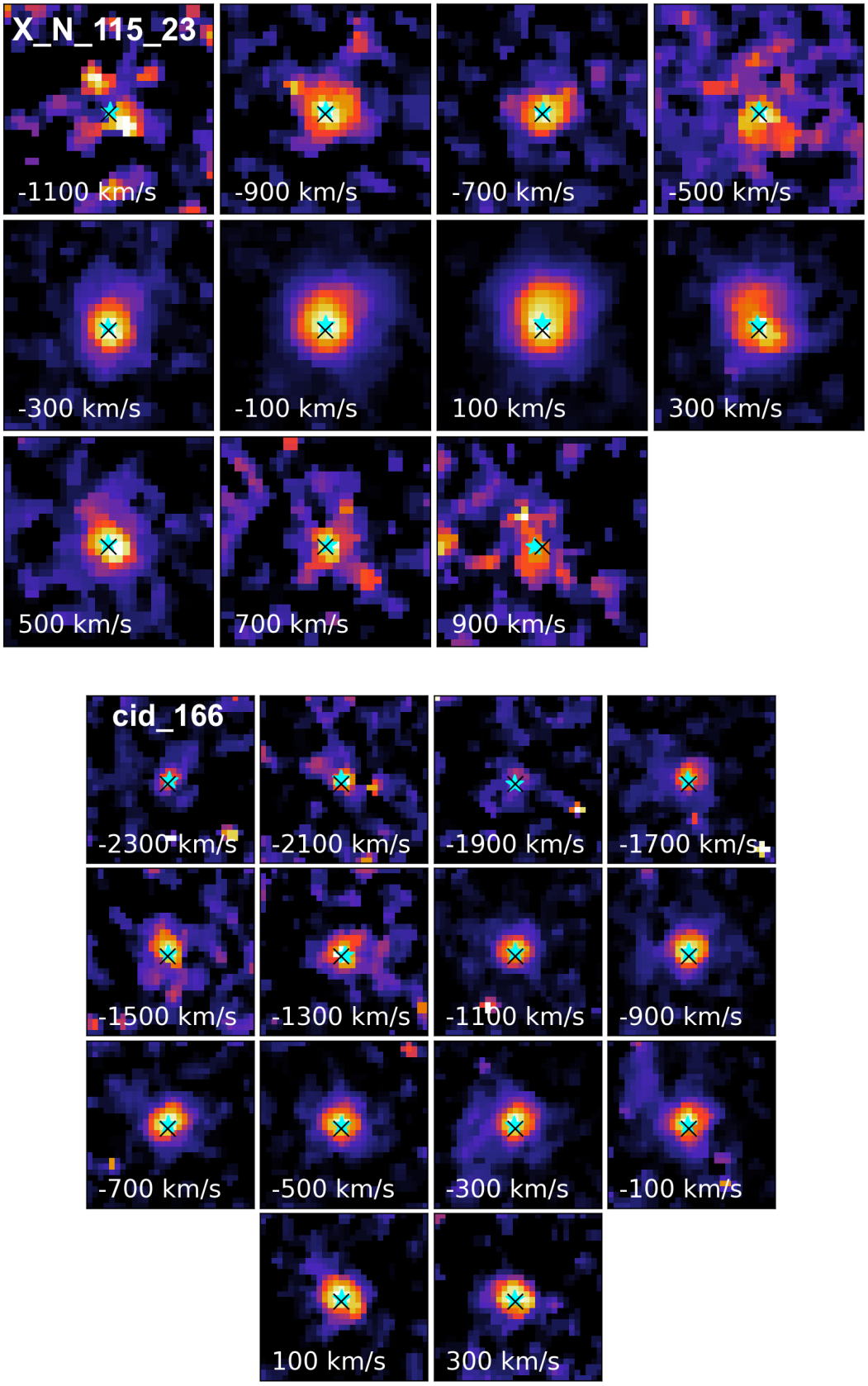

Fig. A.7. Same as in Fig. A.5 for X_N_115_23 and cid_166.

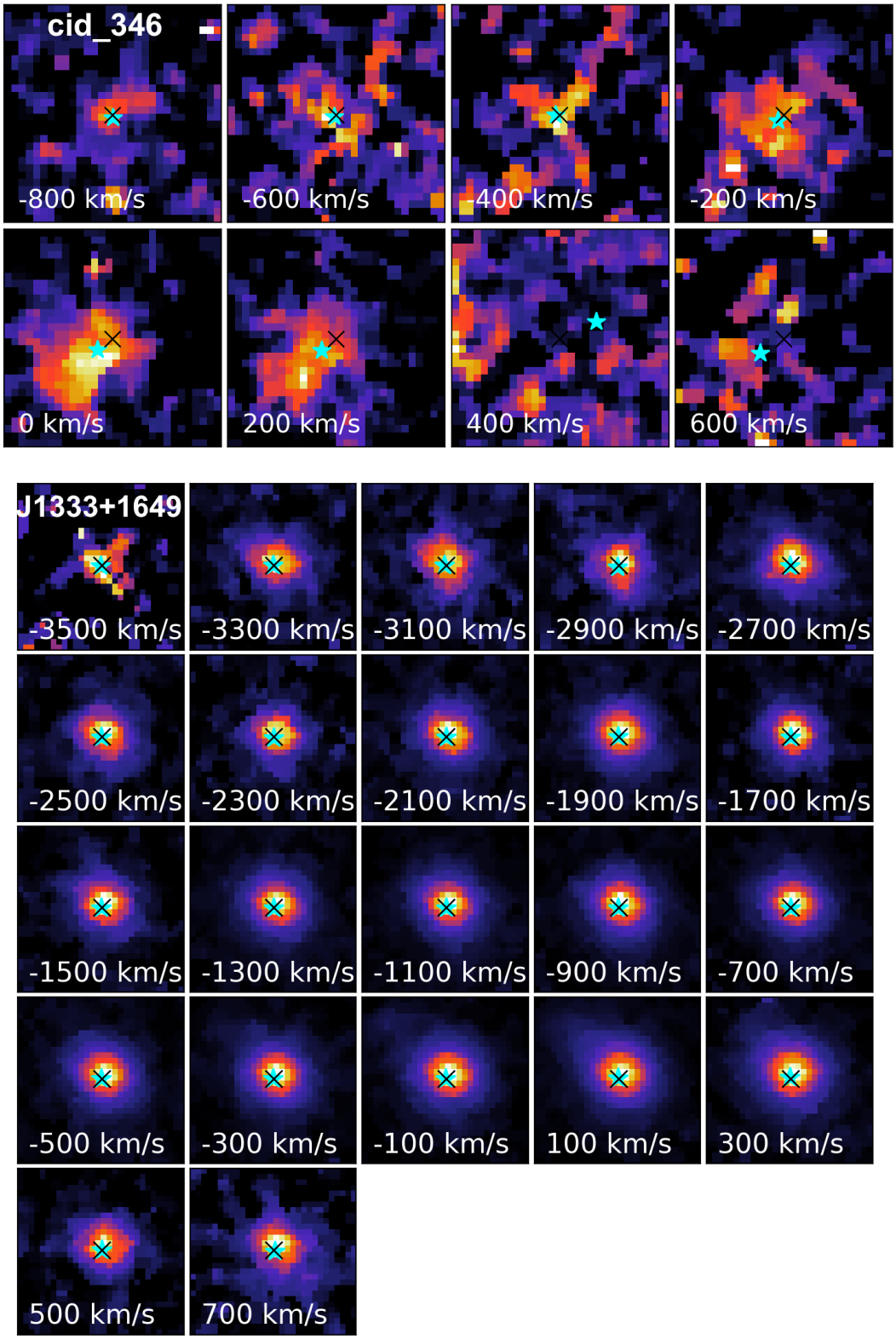

Fig. A.8. Same as in Fig. A.5 for cid_346 and J1333+1649.

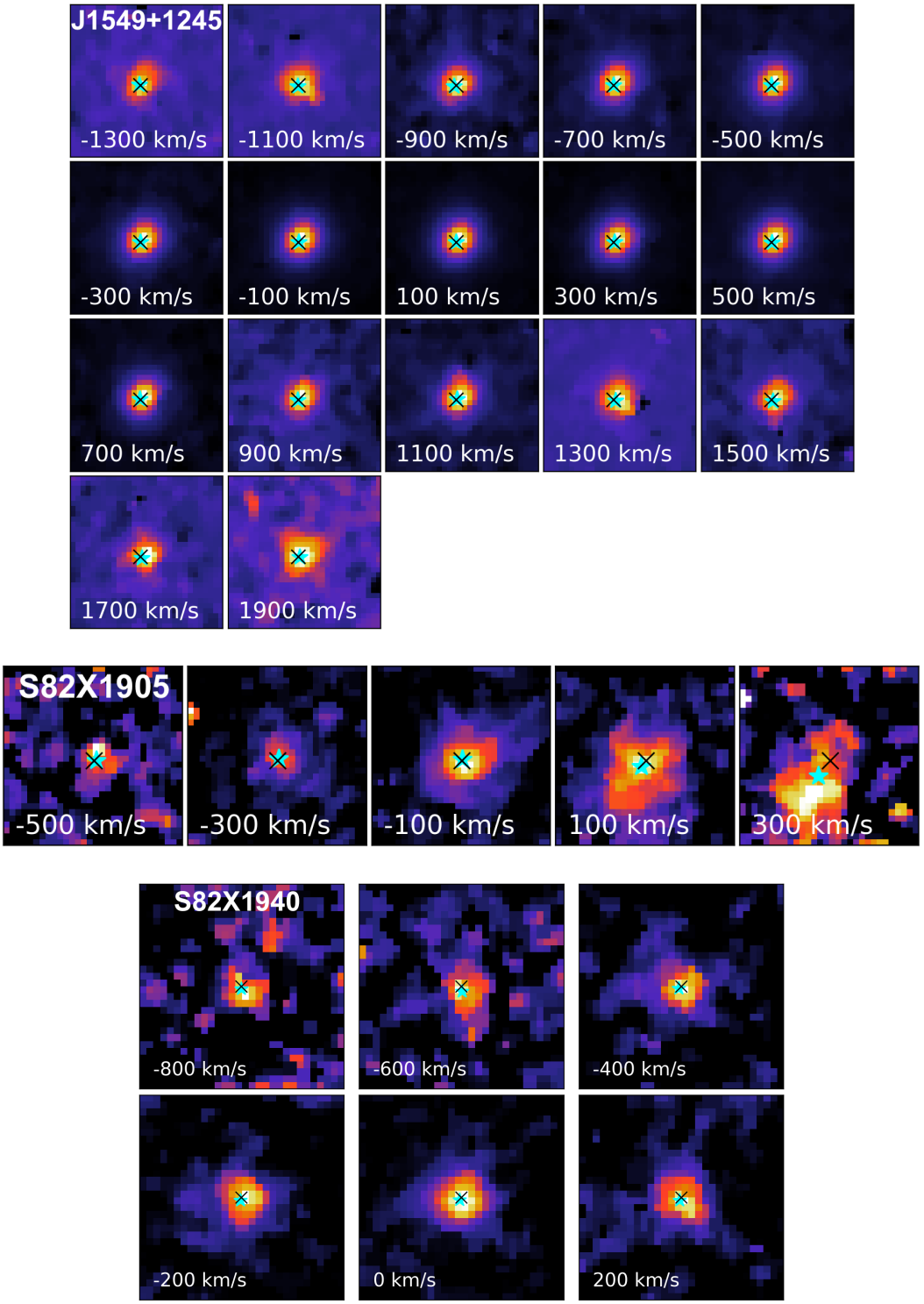

Fig. A.9. Same as in Fig. A.5 for J1549+1245, S82X1905, and S82X1940.